Received: 5 August 2021 | Accepted: 16 August 2021

DOI: 10.1002/jcb.30142

RESEARCH ARTICLE

Journal of Cellular Biochemistry WILEY

Computational decomposition reveals reshaping of the SARS-CoV-2–ACE2 interface among viral variants expressing the N501Y mutation

Eileen Socher[1,2] | **Marcus Conrad**[3] | **Lukas Heger**[4] | **Friedrich Paulsen**[1,5] | **Heinrich Sticht**[3,6] | **Friederike Zunke**[7] | **Philipp Arnold**[1]

[1]Functional and Clinical Anatomy, Institute of Anatomy, Friedrich-Alexander University Erlangen-Nürnberg (FAU), Erlangen, Germany

[2]Institute for Clinical and Molecular Virology, University Hospital Erlangen, Friedrich-Alexander University Erlangen-Nürnberg (FAU), Erlangen, Germany

[3]Division of Bioinformatics, Institute of Biochemistry, Friedrich-Alexander University Erlangen-Nürnberg (FAU), Erlangen, Germany

[4]Department of Dermatology, Laboratory of Dendritic Cell Biology, University Hospital Erlangen, Friedrich-Alexander University Erlangen-Nürnberg (FAU), Erlangen, Germany

[5]Department of Operative Surgery and Topographic Anatomy, Sechenov University, Moscow, Russia

[6]Erlangen National High Performance Computing Center (NHR@FAU), Friedrich-Alexander University Erlangen-Nürnberg (FAU), Erlangen, Germany

[7]Department of Molecular Neurology, University Hospital Erlangen, Friedrich-Alexander University Erlangen-Nürnberg (FAU), Erlangen, Germany

Correspondence: Eileen Socher and Philipp Arnold, Institute of Anatomy, Functional and Clinical Anatomy, Friedrich-Alexander University Erlangen-Nürnberg (FAU), Universitätsstraße 19, 91054 Erlangen, Germany.
Email: eileen.socher@fau.de and philipp.arnold@fau.de

Abstract

Variants of concern of the SARS-CoV-2 virus with an asparagine-to-tyrosine substitution at position 501 (N501Y) in the receptor-binding domain (RBD) show enhanced infectivity compared to wild-type, resulting in an altered pandemic situation in affected areas. These SARS-Cov-2 variants comprise the two Alpha variants (B.1.1.7, United Kingdom and B.1.1.7 with the additional E484K mutation), the Beta variant (B.1.351, South Africa), and the Gamma variant (P.1, Brazil). Understanding the binding modalities between these viral variants and the host cell receptor ACE2 allows to depict changes, but also common motifs of virus–host cell interaction. The trimeric spike protein expressed at the viral surface contains the RBD that forms the molecular interface with ACE2. All the above-mentioned variants carry between one and three amino acid exchanges within the interface-forming region of the RBD, thereby altering the binding interface with ACE2. Using molecular dynamics (MD) simulations and decomposition of intermolecular contacts between the RBD and ACE2, we identified phenylalanine 486, glutamine 498, threonine 500, and tyrosine 505 as important interface-forming residues across viral variants. However, especially the N501Y exchange increased contact formation for this residue and also induced some local conformational changes.

Comparing here, the in silico generated B.1.1.7 RBD–ACE2 complex with the now available experimentally solved structure reveals very similar behavior during MD simulation. We demonstrate, how computational methods can help to identify differences in conformation as well as contact formation for newly emerging viral variants. Altogether, we provide extensive data on all N501Y expressing SARS-CoV-2 variants of concern with respect to their interaction with ACE2 and how this induces reshaping of the RBD–ACE2 interface.

KEYWORDS

angiotensin-converting enzyme 2 (ACE2), coronavirus, COVID-19, molecular dynamics simulations, SARS-CoV-2, spike protein

1 | INTRODUCTION

The COVID-19 pandemic caused by the SARS-CoV-2 virus is having a major impact on human lives worldwide (World Health Organization https://covid19.who.int).[1] For cellular infection, the virus engages the cell surface protein angiotensin-converting enzyme 2 (ACE2) via its trimeric spike protein.[2,3] Within the spike protein, the receptor-binding domain (RBD) interacts with ACE2[4,5] (Figure 1A), mediating the binding of the virus to the host cell surface. Priming at the S2' cleavage site within the spike protein by the serine protease TMPRSS2 releases the fusion peptide from the protein backbone.[2,6,7] After insertion of the fusion peptide into the host cell membrane and the activation of a conformational switch leading to dissociation of the spike protein's S1 and S2 domains,[1,8,9] the virus and host cell membrane come close and fuse.[2,10] To allow the two membranes to converge, all noncleaved subunits of the spike protein must dissociate from the ACE2 receptors, to avoid steric hindrance.[5,11,12] Thus, optimized binding efficiency between the RBD and ACE2 is important for viral entry.[11] In several viral variants that showed superior infectivity over the wild-type (wt) SARS-CoV-2 virus, amino acid exchanges at the interface of the RBD and ACE2 have been reported (Centers for Disease Control and Prevention (https://www.cdc.gov/coronavirus/2019-ncov/more/science-and-research/scientific-brief-emerging-variants.html); World Health Organization). In this study, we examined the RBDs of the two Alpha variants B.1.1.7 and B.1.1.7 + E484K (both originated in the United Kingdom), the Beta variant B.1.351 (South Africa), and the Gamma variant P.1 (Brazil) in complex with ACE2 using molecular dynamics (MD) simulations. For better distinguishability between the two Alpha variants, we will use the Pango nomenclature (https://cov-lineages.org[13]) for the variants investigated in this study.

The B.1.1.7 variant accommodates an N501Y exchange within the RBD–ACE2 interface, which was previously linked to increased binding to ACE2. For the RBD–ACE2 complex an experimentally solved structure is reported.[3] Moreover, the spike protein holds additional amino acid exchanges that influence the spike protein conformation.[14–16] Within the B.1.1.7 + E484K variant an additional glutamate-to-lysine exchange at position 484 is observed (Centers for Disease Control and Prevention). The B.1.351 and P.1 variants carry both mutations (N501Y and E484K) and have additional exchanges at amino acid position 417: in B.1.351, the lysine at position 417 is exchanged for an asparagine (K417N) and in P.1 for a threonine (K417T) (Centers for Disease Control and Prevention). Notably, the exchange of glutamate for lysine at position 484 is associated with a reduced efficacy for certain vaccines.[17,18]

Here, we demonstrate that progressive viral variants occur with altered patterns of contacts to the human receptor ACE2. Additionally, we show how computational decomposition of the RBD–ACE2 interface can identify residues on the RBD that are critical for virus–host interactions across different SARS-CoV-2 variants. Analyses of contacts between the RBD residues and ACE2 reveal changes in the contact formation pattern that induce a conformational rearrangement of glutamine 498 that is induced by tyrosine 501 in all investigated variants of concerns. The other two sites of mutation at position 484 and 417 influence salt bridge formation and thus change local electrostatic interaction (Figure 1B). Using the experimentally solved structure of the B.1.1.7 RBD with ACE2 (PDB ID code: 7MJN[19]), we could also verify our findings and demonstrate the feasibility of MD simulations to track mutation-induced changes on the structural level.

2 | MATERIALS AND METHODS

2.1 | Generation of the starting structures

To investigate the interface between the RBD of the spike protein and ACE2, the respective wt start structure was taken from the Protein Data Bank (PDB; http://www.rcsb.org/pdb/ PDB ID code: 7KMB.[3] To also generate the starting structures for the MD simulations of the different spike variants, the amino acid substitutions (B.1.1.7: N501Y; B.1.1.7 + E484K: E484K and N501Y; B.1.351: K417N, E484K, and N501Y; P.1: K417T, E484K, and N501Y) were introduced with Swiss-PdbViewer 4.1.0. While we conducted this study, the RBD–ACE2 complex structure with the N501Y mutation (B.1.1.7 variant) was released in the Protein Data Bank with the PDB ID code 7MJN.[19] We used this solved structure for verification of our modeled B.1.1.7 variant.

2.2 | Molecular dynamics simulations

Molecular dynamics simulations were performed using version 20 of the Amber Molecular Dynamics software package (ambermd.org)[20] and the ff14SB force field.[21] Using the Amber Tool LEaP, all systems were electrically neutralized with Na^+ ions and solvated with TIP3P[22] water molecules. The RBD complexed with ACE2 was solvated in a water box with the shape of a truncated octahedron and a distance of at least 25 Å from the borders to the solute.

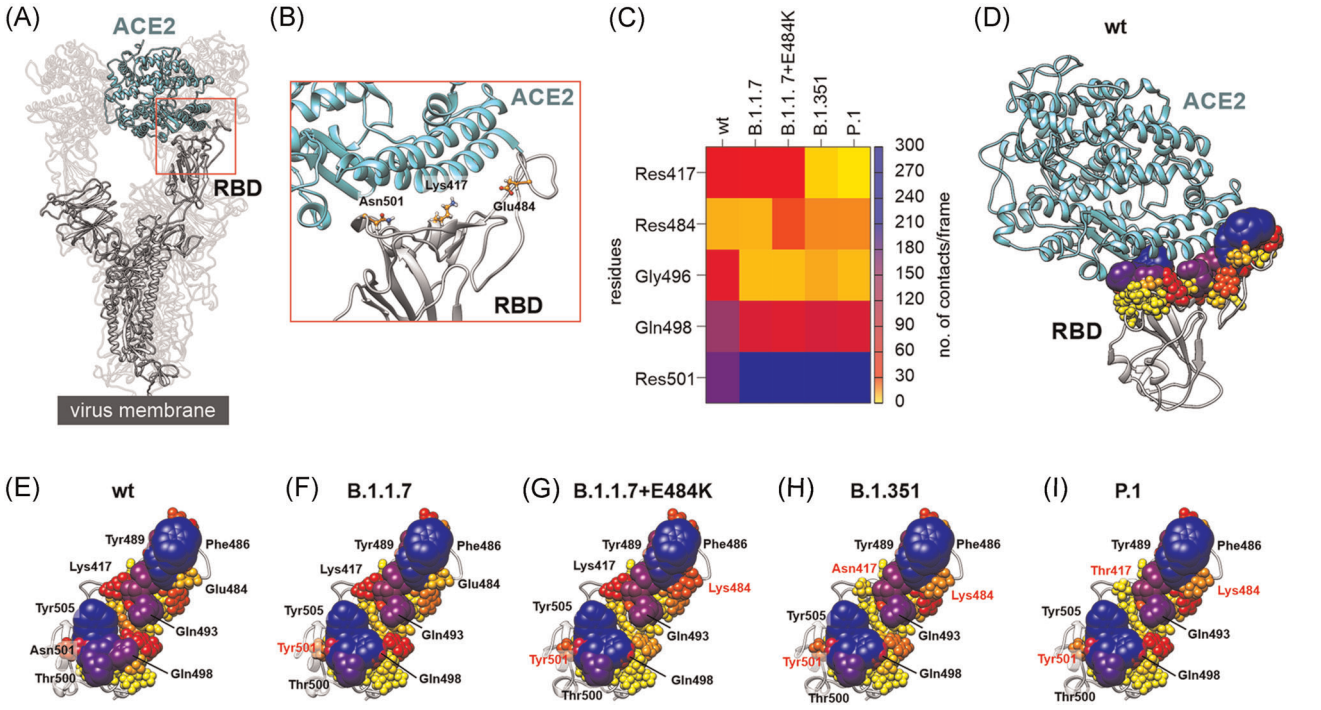

FIGURE 1 Decomposition of contacts. (A) Structural representation of the trimeric spike protein as expressed on the viral membrane (gray) with exposed receptor-binding domain (RBD). The host cell receptor angiotensin-converting enzyme 2 (ACE2) is displayed in aquamarine (PDB ID code: 7KMS[3]). (B) Close up from the interface between the RBD and ACE2. Amino acids mutated in viral variants are depicted with their residues in orange. (C) Heat map of RBD expressed residues important for contacts with ACE2. (D) Wild-type (wt) RBD in complex with ACE2 (aquamarine). All residues within a maximum distance of 8 Å to ACE2 are displayed according to their number of contacts with different colors and sphere radii. (E) View on the interface formed by the wt RBD with residues displayed in different colors and sphere diameters according to their contact numbers (color code as in C). Especially lysine 417 (Lys417), glutamate 484 (Glu484), phenylalanine 486 (Phe486), tyrosine 489 (Tyr498), glutamine 498 (Gln498), threonine 500 (Thr500), asparagine 501 (Asn501), and tyrosine 505 (Tyr505) were of interest. (F) View on the interface formed by the RBD of the B.1.1.7 variant with ACE2. Note that residue 501 is mutated to tyrosine (Tyr501; red) in this variant. (G) View on the interface formed by the RBD of the B.1.1.7 + E484K variant with ACE2. Note the additional change of residue 484 from glutamate to lysine (Lys484; red) compared to wt and B.1.1.7. (H) View on the interface formed by the RBD of the B.1.351 variant with ACE2. This variant carries the tyrosine at position 501, the lysine at position 484, and an additional exchange from lysine to asparagine at position 417 (Asn417; red). (I) View on the interface formed by the RBD of the P.1 variant with ACE2. Besides a tyrosine at position 501 and a lysine at position 484 this variant carries a lysine to threonine exchange at position 417 (Thr417; red)

The simulations followed a previously applied protocol.[23] First, minimization was carried out in three consecutive steps to optimize the geometry of the initial structures. In the first step of the minimization, the water molecules were minimized, while all other atoms were restrained at the initial positions with a constant force of 10 kcal mol^{-1} $Å^{-2}$. In the second step, additional relaxation of the sodium ions and the hydrogen atoms of the protein was allowed, while the remaining protein was restrained with 10 kcal mol^{-1} $Å^{-2}$. In the last step, no restraints were used, so the entire protein, ions, and water molecules were minimized. All three minimization parts started with 2500 steps using the steepest descent algorithm, followed by 2500 steps of a conjugate gradient minimization. After minimization, the systems were equilibrated in two successive steps. In the first step, the temperature was increased from 10 to 310 K within 0.1 ns and the protein was restrained with a constant force of 5 kcal mol^{-1} $Å^{-2}$. In the second step (0.4 ns length), only the Cα atoms of the protein were restrained with a constant force of 5 kcal mol^{-1} $Å^{-2}$. In both equilibration steps, the time step was 2 fs. Minimization and equilibration were carried out on CPUs, while the subsequent production runs were performed using pmemd.CUDA on Nvidia A100 GPUs.[24–26] Subsequent 500 ns long production runs were performed without any restraints and at 310 K (regulated by a Berendsen thermostat.[27] Furthermore, the constant pressure periodic boundary conditions with an average pressure of 1 bar and isotropic position scaling were used. For bonds involving hydrogen, the SHAKE algorithm[28] was applied in the equilibration and production phases. To accelerate the production phase of the MD simulations, hydrogen mass repartitioning[29] was used in combination with a time step of 4 fs. For all different spike protein variants in complex with ACE2, the MD simulations were performed four times.

Trajectory analysis (analysis of root-mean-square fluctuations (RMSF), analysis of contacts (always with distance criterion of ≤5 Å between any pair of atoms; total fraction of contacts for residue pairs), measurement of interatomic distances, calculation of linear interaction energy (LIE; electrostatic interactions) was performed using the Amber tool cpptraj.[30] The in silico alanine scan was done by the program foldx 5,[31] specifically by its PSSM algorithm. The depicted ΔΔG values describe the loss or gain in energy from the interaction between the SARS-CoV-2 spike RBD and ACE2 as a result of a mutation to alanine. Positive values are indicating a destabilization of the interface upon the alanine mutation, which vice versa implies that the original residue acted more stabilizing.

2.3 | Statistics and display

Statistical analyses were performed with GraphPad Prism (version 8.0.0 for Windows; GraphPad Software, www.graphpad.com) and statistical tests were applied as indicated below the figure. Plots were created in GraphPad and Gnuplot (version 5.2). All structure images were made with UCSF Chimera 1.15.[32]

3 | RESULTS AND DISCUSSION

3.1 | Mutations reorganize contact formation pattern between RBD and ACE2

To calculate contact formation between the cell surface receptor ACE2 and different RBD variants, the structure of the wt RBD and ACE2 complex (PDB ID code: 7KMB[3]) was used as starting point. Variant-specific amino acid substitutions were introduced in the RBD sequence before applying MD simulations: B.1.1.7 (N501Y), B.1.1.7 + E484K (N501Y, E484K), B.1.351 (N501Y, E484K, K417N), and P.1 (N501Y, E484K, K417T). After four independent simulation runs for 500 ns, we decomposed the number of contacts per residue for residues expressed on the RBD within the interface with ACE2 (all distances below 5 Å counted as contact; Figure S1A). We found many amino acids with unchanged contacts and also some with a very high number of contacts that showed no difference (Figure S1A). These include for example phenylalanine 486, tyrosine 489, threonine 500, and tyrosine 505 and were also identified by other groups before.[33] Taking a closer look at the positions that carry mutations, intriguing differences in contact formation could be observed. While a reduction was seen for changes at position 417, where a lysine is exchanged to an asparagine (B.1.351) or a threonine (P.1), increased number of contacts were detected for E484K and N501Y mutations (Figure 1C). The increase in contacts at position 501 when tyrosine is present might also explain an overall stronger interaction as deduced from experimental data.[34–37] Interestingly, we also identified changes in contact formation for residues that were not mutated but reported with constantly lower contact numbers in all N501Y carrying variants (Figure 1C). These include glycine 496 and glutamine 498 (Figure 1C). As expected those residues within close proximity of ACE2 form a large number of contacts (Figure 1D). However, differences can be found in individual side-by-side comparisons of the different variants (Figure 1E–I). Our analysis indicates a rearrangement of contacts between the RBD and ACE2 with a distinct increase in contact formation for individual RBD residues and a loss of contacts for others. Thus, this reshaping of the contacts seems to induce a stronger interaction between the

RBD and ACE2. Gain and loss of contacts seem to happen in a balanced matter as the need for dissociation is also a driving force for viral evolution.[38,39] To mirror and recapitulate the increase in interaction energy, we performed in silico alanine scans for position 501 in wt and B.1.1.7 RBD–ACE2 complexes. These two variants were chosen, to directly compare the effect of the N501Y exchange and exclude influences caused by additional mutations within the RBD. Calculation of the ΔΔG value showed a stronger contribution to binding energy for tyrosine at position 501 when compared to asparagine (Figure S1B) and thus fits well to experimental data.[34–37] We also analyzed the RMSF values for the RBD residues and found no significant changes for any of the variants analyzed (Figure S1C).

3.2 | The N501Y mutation induces a local conformational rearrangement

To understand the increased number of contacts formed by tyrosine 501 when compared to asparagine 501, we looked at neighboring amino acids at the interaction interface of the RBD and ACE2 (Figure 2A). Bulk comparison of the asparagine (wt) or a tyrosine (all analyzed variants) at position 501 shows a significant increase in the number of contacts per frame for tyrosine (Figure 2B). Further decomposition of the contacts to individual residues expressed on ACE2 shows an increase in contacts with residues tyrosine 41 and lysine 353 for a tyrosine residue at RBD position 501 (Figure 2C). The increase in contacts with tyrosine 41 might also induce π-electron stacking and might be responsible for the overall increase in interaction energy as speculated before.[40] Importantly, free energy calculations such as MM/GBSA might not pick up this increased binding energy and erroneously come up with reduced interaction energies.

Our contact analysis also revealed a reduced number of contacts for glutamine 498, which is in close proximity to residue 501 (Figure 2A). Here, bulk analysis of wt against tyrosine expressing variants showed a reduction of contacts for glutamine 498 by more than half (Figure 2D). To further detect changes on the individual amino acid level, we also decomposed the interaction regime of glutamine 498 and identified reduced interaction with the ACE2 residues aspartate 38, tyrosine 41, and lysine 353. We suggest two reasons that might explain the reduction in contact formation. First, the bulkier tyrosine side chain expels glutamine 498 from the interaction interface and second, a tyrosine at position 501 claims especially tyrosine 41 and lysine 353 as interaction partners for itself. As we are well aware that the modeled start conformation might introduce a certain amount of uncertainty, when introducing amino acid exchanges, we also made use of the experimentally solved structure of the B.1.1.7 RBD in complex with ACE2 (PDB ID code: 7MJN[19]). Using this experimentally determined complex structure as starting model, we also performed four independent MD simulation runs of 500 ns and compared the results to our data based on the wt structure with "modeled" amino acid exchanges. First of all, we compared the experimentally solved structure with the B.1.1.7 variant (PDB ID code: 7MJN[19]) to this here in silico generated B.1.1.7 structure. They both show a very good overall overlay, especially for glutamine 498 and tyrosine 501 (Figure S2A). In all other analyses, the experimentally solved B.1.1.7 structure (PDB ID code: 7MJN[19]) and our in silico derived model behaved nearly identical. They showed the same number of contacts formed by tyrosine 501 (Figure S2B,C) and for contacts formed by glutamine 498 (Figure S2D,E). Thus, we conclude that the in silico produced models are very close to the experimentally derived structure in terms of contact formation properties and might be helpful tools to gain fast insight into property changes induced by newly emerging mutations at the RBD–ACE2 interface.

3.3 | The E484K mutation induces salt bridge formation with the ACE2 glutamate 75

In the decomposed contact analyses, we also identified an increased number of contacts to ACE2 for the residue at position 484 after insertion of a lysine for the glutamate (E484K, Figure 1C). The same was confirmed in our bulk analysis when we compared variants with a glutamate (wt, B.1.1.7) to those with a lysine (B.1.1.7 + E484K, B.1.351, P.1) at position 484 and further identified increased contact formation for lysine (Figure 3A). Decomposition of the interactome to individual residues showed an increased contact formation with glutamate 75 from ACE2 (Figure 3B). This glutamate 75 is expressed on a neighboring helix of ACE2 and is at a good distance for salt bridge formation (Figure 3C,D). To further capitalize on this point, we analyzed the distance between the nitrogen atom in zeta position of lysine 484 (RBD) as well as the carbon atom in delta position of glutamate 75 (ACE2) and found both in a salt bridge favored distance below 4 Å in a considerably amount of the simulation time (example shown in Figure 3D). We also used the LIE values for the electrostatic interaction of residue 484 with ACE2 and compared them in a bulk approach for variants with a glutamate to those with a lysine and found a significant increase (Figure 3E). From these results, we conclude that an additional salt bridge can be formed between lysine 484 from the RBD and glutamate 75 from ACE2. This might stabilize the loop that holds residue 484 and increase the local stability.

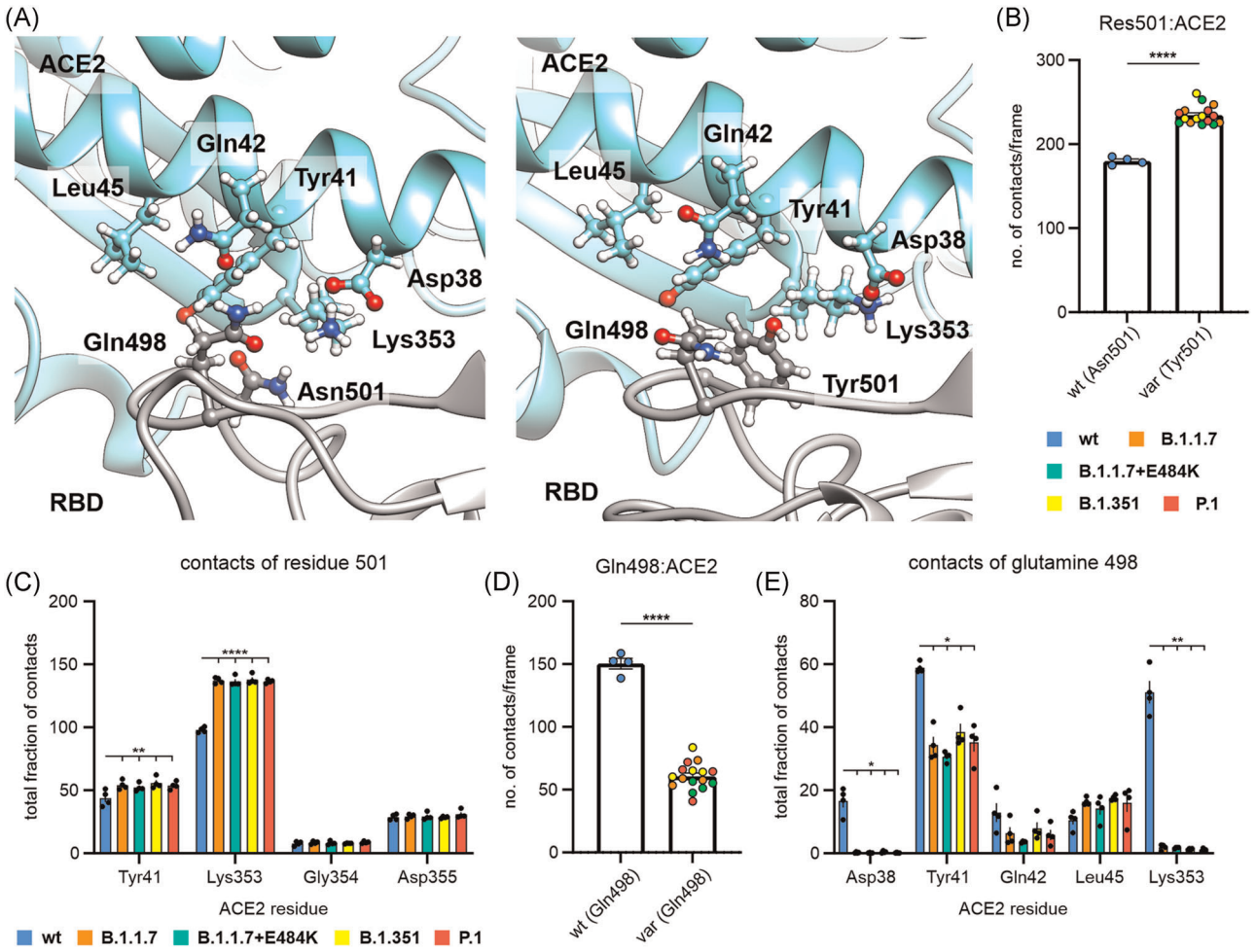

FIGURE 2 Contact formation around residue 501. (A) Left panel: Structural representation of an asparagine 501 expressing wild-type (wt) receptor-binding domain (RBD, gray) in complex with angiotensin-converting enzyme 2 (ACE2) (aquamarine). The ACE2 residues aspartate 38 (Asp38), tyrosine 41 (Tyr41), glutamine 42 (Gln42), leucine 45 (Leu45), and lysine 353 (Lys353) were potential interactors for glutamine 498 (Gln498). Gln498 was in close proximity of RBD asparagine 501. The right panel shows a structural representation of a tyrosine 501 expressing variant of the RBD in complex with ACE2. ACE2 residues tyrosine 41 (Tyr41), glutamine 42 (Gln42), and leucine 45 (Leu45) present potential interactors for glutamine 498 (Gln498). The bulky tyrosine 501 seemed to partially exclude glutamine 498 from the RBD-ACE2 interface. (B) Number of contacts per frame formed by residue 501 comparing asparagine (wt) and tyrosine (all others) expressing variants in bulk analysis. Different colors represent the different variants and statistical analysis was performed using unpaired Student's *t* test with $^{****}p < .0001$. (C) Decomposition of residue 501 contacts to residues expressed on ACE2. All variants expressing a tyrosine at position 501 show significantly increased contact formation with tyrosine 41 (Tyr41) and lysine 353 (Lys353) when compared to wt. Statistical analysis was performed using two-way analysis of variance (ANOVA) ($n = 4$, differences assumed significant for $^{**}p < .01$ and $^{****}p < .0001$, lowest significance in group is shown in graph, individual values can be found in Table S1). (D) Bulk analysis for all contacts formed by glutamine 498 (Gln498) shows significantly lower numbers for variants expressing a tyrosine at position 501. Different colors represent the different variants and statistical analysis was performed using an unpaired Student's *t* test with $^{****}p < .0001$.
(E) Decomposition of the interaction of glutamine 498 with residues expressed on ACE2. Significant reduction in contact number is seen for aspartate 38 (Asp38), tyrosine 41 (Tyr41), and lysine 353 (Lys353). Statistical analysis was performed using two-way ANOVA ($n = 4$, differences assumed significant for $^{*}p < .05$ and $^{**}p < .01$, lowest significance in group is shown in graph, individual values can be found in Table S1)

3.4 | The K417N/T mutation destroys a salt bridge between the RBD and aspartate 30 of ACE2

For residue 417 we found a strong decrease in contact formation in variants where lysine was exchanged to asparagine (B.1.351) or threonine (P.1). Bulk analysis showed that all other variants showed a comparable number of contacts per frame (Figure 4A). Decomposition of the interactions to individual residues revealed that contacts with aspartate 30 expressed on ACE2 are lost (Figure 4B). Both residues are in close

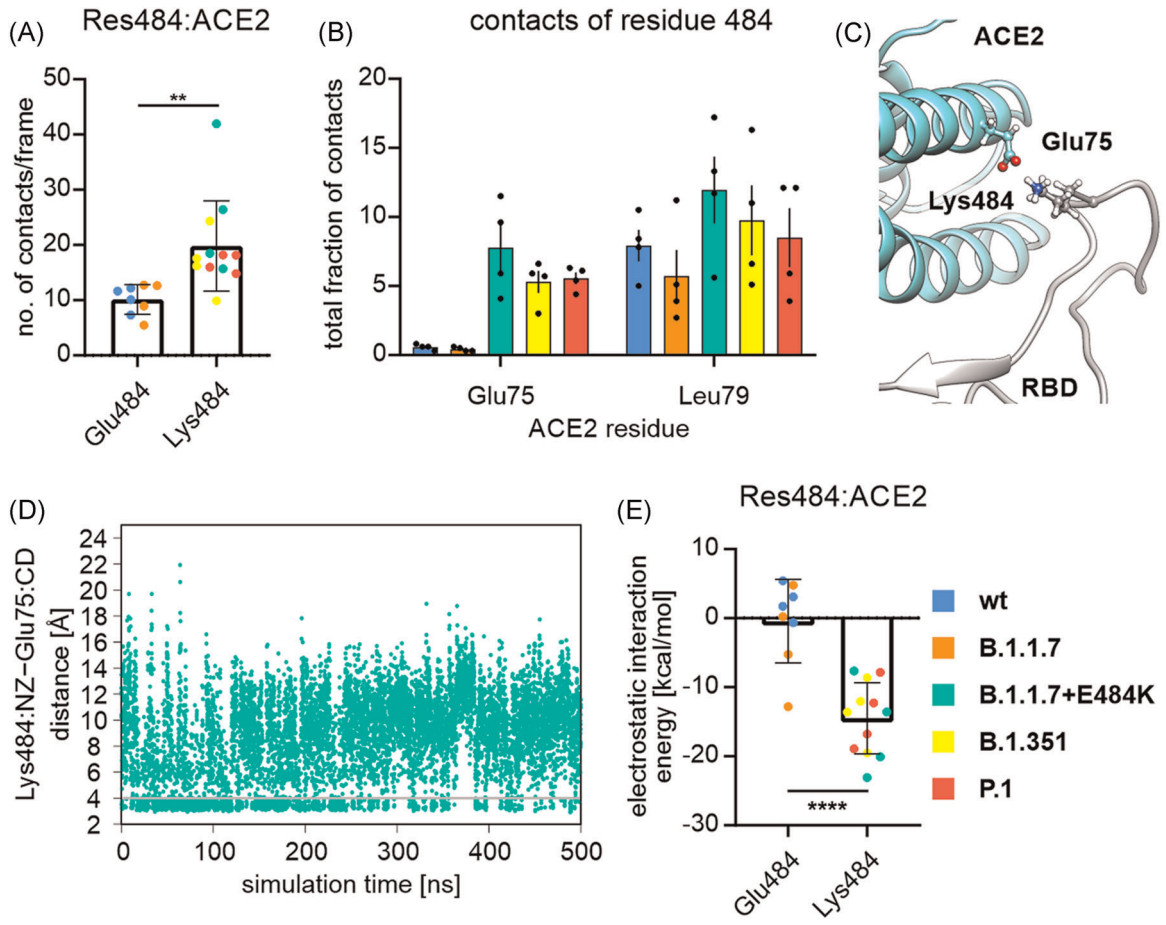

FIGURE 3 The E484K mutation leads to a new salt bridge with glutamate 75 from angiotensin-converting enzyme 2 (ACE2). (A) Average number of contacts per frame for residue 484 to ACE2. The number is significantly higher for variants that express a lysine (B.1.1.7 + E484K: green, B.1.351: yellow, and P.1: red) compared to those expressing glutamate (wild-type (wt): blue, and B.1.1.7: orange; Student's two-tailed *t* test; $^{**}p < .01$). (B) Decomposition of contacts for residue 484 (glutamate or lysine) with glutamate 75 (Glu75) or leucine 79 (Leu79) expressed on ACE2. (C) Structural representation of lysine 484 (Lys484) as expressed on the RBD of B.1.1.7 + E484K, B.1.351 and P.1, and glutamate 75 (Glu75) expressed on ACE2. (D) Exemplary distance plot for the zeta-N-atom of lysine 484 of B.1.1.7 + E484K to the delta-C-atom of glutamate 75 expressed on ACE2. (E) Electrostatic linear interaction energy compared between variants that express a lysine (B.1.1.7 + E484K: green, B.1.351: yellow, and P.1: red) or a glutamate (wt: blue and B.1.1.7: orange) at position 484 (Student's two-tailed *t* test; $^{****}p < .0001$)

proximity (Figure 4C) and distance plotting between the nitrogen atom in zeta position from lysine and the carbon atom in gamma position from aspartate showed both in a salt bridge favored distance of 4 Å or below for variants that express a lysine at position 417 (Figure 4D, example shown for wt). In line with contact and distance plots, we also found the electrostatic part of the LIE measured between residue 417 and ACE2 drastically reduced when lysine was exchanged for an asparagine or threonine (Figure 4E). Thereby, we conclude that loss of lysine at position 417 also abrogates salt bridge formation at this position. Interestingly, the K417N/T mutation is only seen in variants that also carry the E484K mutation (e.g., www.rki.de). Thus, the salt bridge formed by lysine 484 and glutamate 75 might compensate for the loss of the salt bridge formed by lysine 417 and aspartate 30. A driving force for selection of this variant might be the increased expression of the RBD, that was measured in a yeast system when lysine 417 was exchanged.[36]

4 | CONCLUSIONS

Newly emerging viral variants of SARS-CoV-2 often dominate the pandemic before experimental structural data is available, to determine effects on conformation and/or interaction with ACE2. Thus, MD simulation holds great potential to assist in the curation of such data and thereby help to identify key changes in conformation and structural dynamics. Using the experimentally solved structure of the B.1.1.7 RBD in complex with ACE2 (PDB ID code: 7MJN) to

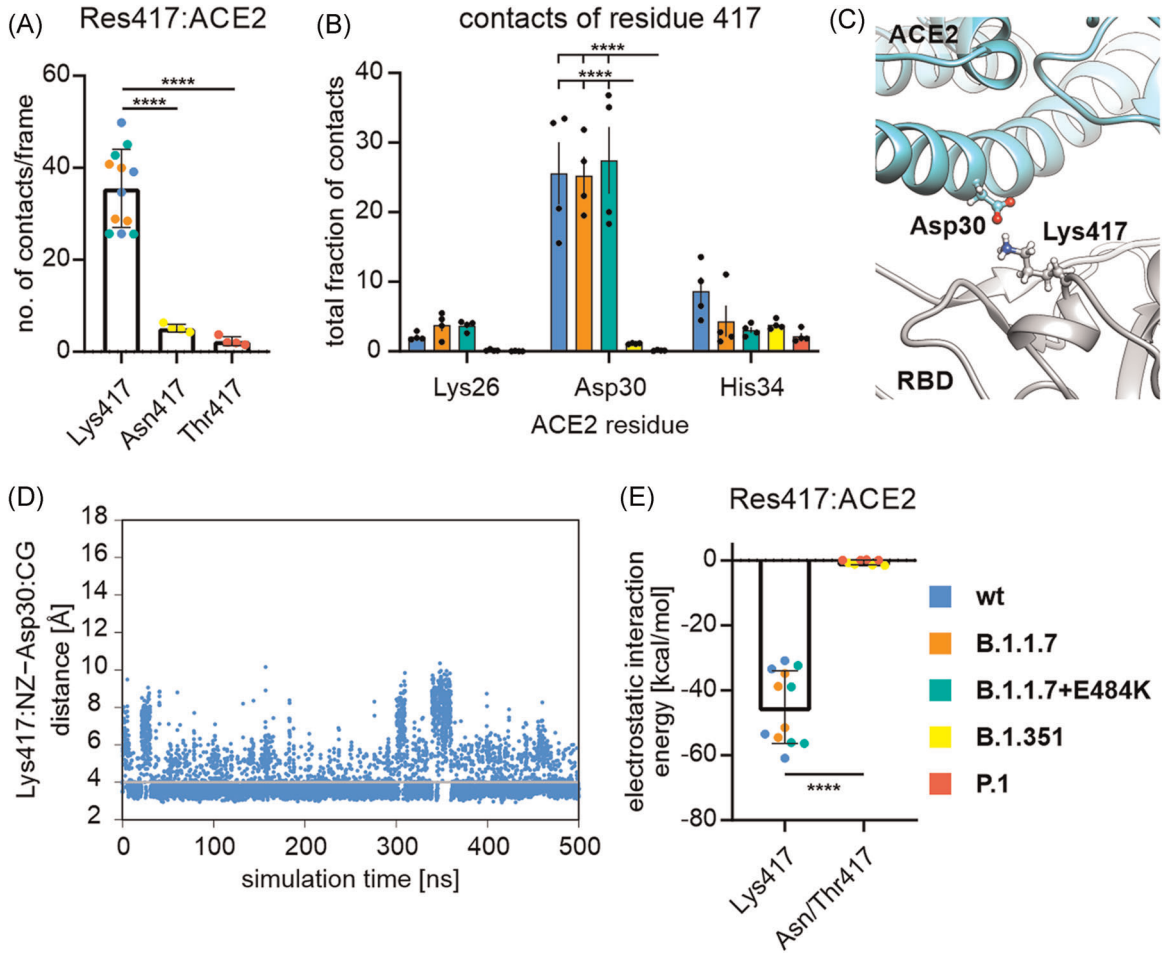

FIGURE 4 Exchange of lysine 417 to asparagine or threonine abrogates salt bridge formation. (A) Average number of contacts per frame for residue 417 to angiotensin-converting enzyme 2 (ACE2). In variants that express a lysine at this position (wild-type (wt): blue, B.1.1.7: orange and B.1.1.7 + E484K: green) this number is significantly higher when compared to variants with an asparagine (B.1.351: yellow) or threonine (P.1: red; one-way analysis of variance [ANOVA]; $n = 4$ or 12; ****$p < .0001$). (B) Decomposition of the contact formation of residue 417 shows significantly reduced contacts with aspartate 30 (Asp30) expressed on ACE2 in variants that express an asparagine (B.1.351) or a threonine (P.1). Statistical analysis was performed using two-way ANOVA ($n = 4$, differences assumed significant for ****$p < .0001$). (C) Structural representation of the salt bridge formed by lysine 417 from the receptor-binding domain (RBD) (Lys417) and aspartate 30 from ACE2 (Asp30). (D) Exemplary distance plot for a simulation from the wt RBD with ACE2 over time, for lysine 417 and aspartate 30. The gray line indicates a distance of 4 Å. (E) Electrostatic linear interaction energy compared between RBD variants with a lysine (wt: blue, B.1.1.7: orange and B.1.1.7 + E484K: green) or asparagine/threonine (B.1.351: yellow and P.1: red; Student's two-tailed t test; ****$p < .0001$)

validate our simulated data, we showed the reliability of computational approaches. Thus, we believe that MD simulation holds the potential (especially with continuously increasing computer power) to follow structural changes in "real-time" and identify common trends among emerging viral variants. Here, we show that all variants that carry the N501Y mutation reshape the pattern of contacts with ACE2. Here, decomposition of the contacts to individual amino acids highlighted the importance of single amino acids (and their exchange) for interface formation. Together, the N501Y carrying variants demonstrate higher binding efficacy with a few changes in contact formation, which leads to a stronger interaction with ACE2. Future studies will show how all these variants of concern (carrying the N501Y mutation) compare to the Delta variant of SARS-CoV-2. Interestingly, this variant does not carry the N501Y mutation but dominates the pandemic. Our results and data from other groups indicate that MD simulation is a powerful tool to evaluate the consequences of individual amino acid exchanges on the interaction energies between the RBD and ACE2 and beyond.[42,43]

ACKNOWLEDGMENTS

The authors gratefully acknowledge the computing resources and support provided by the Erlangen Regional Computing Center (RRZE) and by NHR@FAU.

CONFLICT OF INTERESTS

The authors declare that there are no conflict of interests.

AUTHOR CONTRIBUTIONS

Eileen Socher, Friederike Zunke, and Philipp Arnold conceived the study; Eileen Socher conducted the MD simulations; Eileen Socher, Marcus Conrad, and Philipp Arnold performed data analysis; Eileen Socher, Lukas Heger, and Philipp Arnold generated visualization of the data; Eileen Socher, Heinrich Sticht, Friedrich Paulsen, Friederike Zunke, and Philipp Arnold contributed to the design of the study as well as discussion of the data; Eileen Socher, Friederike Zunke, and Philipp Arnold wrote the initial draft; all authors reviewed the manuscript before submission.

DATA AVAILABILITY STATEMENT

Data will be available upon request.

ORCID

Eileen Socher https://orcid.org/0000-0002-6239-3749
Marcus Conrad https://orcid.org/0000-0002-6352-9046
Lukas Heger https://orcid.org/0000-0001-5591-2187
Friedrich Paulsen https://orcid.org/0000-0002-0527-0953
Heinrich Sticht https://orcid.org/0000-0001-5644-045X
Friederike Zunke https://orcid.org/0000-0002-0408-6388
Philipp Arnold https://orcid.org/0000-0003-3273-9865

REFERENCES

1. Chen, N, Zhou M, Dong X, et al. Epidemiological and clinical characteristics of 99 cases of 2019 novel coronavirus pneumonia in Wuhan, China: a descriptive study. *The Lancet*. 2020;395(10223):507-513. https://doi.org/10.1016/S0140-6736(20)30211-7
2. Hoffmann M, Kleine-Weber H, Schroeder S, et al. SARS-CoV-2 cell entry depends on ACE2 and TMPRSS2 and is blocked by a clinically proven protease inhibitor. *Cell*. 2020;181(2):271-280. https://doi.org/10.1016/j.cell.2020.02.052
3. Zhou, T, Tsybovsky Y, Gorman J, et al. Cryo-EM structures of SARS-CoV-2 spike without and with ACE2 reveal a pH-dependent switch to mediate endosomal positioning of receptor-binding domains. *Cell Host Microbe*. 2020;28(6):867-879. https://doi.org/10.1016/j.chom.2020.11.004
4. Cao W, Dong C, Kim S, et al. Biomechanical characterization of SARS-CoV-2 spike RBD and human ACE2 protein-protein interaction. *Biophys J*. 2021;120:1011-1019. https://doi.org/10.1016/j.bpj.2021.02.007
5. Yang, J, Petitjean S, Koehler M, et al. Molecular interaction and inhibition of SARS-CoV-2 binding to the ACE2 receptor. *Nat Commun*. 2020;11(1):4541. https://doi.org/10.1038/s41467-020-18319-6
6. Hoffmann M, Kleine-Weber H, Pöhlmann S. A multibasic cleavage site in the spike protein of SARS-CoV-2 is essential for infection of human lung cells. *Mol Cell*. 2020;78(4):779-784. https://doi.org/10.1016/j.molcel.2020.04.022
7. Simmons G, Zmora P, Gierer S, Heurich A, Pöhlmann S. Proteolytic activation of the SARS-coronavirus spike protein: cutting enzymes at the cutting edge of antiviral research. *Antiviral Res*. 2013;100(3):605-614. https://doi.org/10.1016/j.antiviral.2013.09.028
8. Belouzard S, Chu VC, Whittaker GR. Activation of the SARS coronavirus spike protein via sequential proteolytic cleavage at two distinct sites. *Proc Natl Acad Sci U S A*. 2009;106(14):5871-5876. https://doi.org/10.1073/pnas.0809524106
9. Millet JK, Whittaker GR. Host cell entry of Middle East respiratory syndrome coronavirus after two-step, furin-mediated activation of the spike protein. *Proc Natl Acad Sci U S A*. 2014;111(42):15214-15219. https://doi.org/10.1073/pnas.1407087111
10. Matsuyama S, Ujike M, Morikawa S, Tashiro M, Taguchi F. Protease-mediated enhancement of severe acute respiratory syndrome coronavirus infection. *Proc Natl Acad Sci U S A*. 2005;102(35):12543-12547. https://doi.org/10.1073/pnas.0503203102
11. Benton DJ, Wrobel AG, Xu P, et al. Receptor binding and priming of the spike protein of SARS-CoV-2 for membrane fusion. *Nature*. 2020;588(7837):327-330. https://doi.org/10.1038/s41586-020-2772-0
12. Ni D, Lau K, Lehmann F, et al. Structural investigation of ACE2 dependent disassembly of the trimeric SARS-CoV-2 spike glycoprotein. *bioRxiv*. 2020. https://doi.org/10.1101/2020.10.12.336016
13. Rambaut A, Holmes EC, O'Toole Á, et al. A dynamic nomenclature proposal for SARS-CoV-2 lineages to assist genomic epidemiology. *Nat Microbiol*. 2020;5(11):1403-1407. https://doi.org/10.1038/s41564-020-0770-5
14. Harvey WT, Carabelli AM, Jackson B, et al. SARS-CoV-2 variants, spike mutations and immune escape. *Nat Rev Microbiol*. 2021;19(7):409-424. https://doi.org/10.1038/s41579-021-00573-0
15. Mohammad A, Abubaker J, Al-Mulla F. Structural modelling of SARS-CoV-2 alpha variant (B.1.1.7) suggests enhanced furin binding and infectivity. *Virus Res*. 2021;303:198522. https://doi.org/10.1016/j.virusres.2021.198522
16. Socher E, Conrad M, Heger L, et al. Mutations in the B.1.1.7 SARS-CoV-2 spike protein reduce receptor-binding affinity and induce a flexible link to the fusion peptide. *Biomedicines*. 2021;9(5):525. https://doi.org/10.3390/biomedicines9050525
17. Jangra S, Ye C, Rathnasinghe R, et al. The E484K mutation in the SARS-CoV-2 spike protein reduces but does not abolish neutralizing activity of human convalescent and post-vaccination sera. *medRxiv*. 2021. https://doi.org/10.1101/2021.01.26.21250543
18. Weisblum Y, Schmidt F, Zhang F, et al. Escape from neutralizing antibodies by SARS-CoV-2 spike protein variants. *eLife*. 2020;9:e61312. https://doi.org/10.7554/eLife.61312
19. Zhu X, Mannar D, Srivastava SS, et al. Cryo-electron microscopy structures of the N501Y SARS-CoV-2 spike protein in complex with ACE2 and 2 potent neutralizing antibodies. *PLOS Biol*. 2021;19(4):e3001237. https://doi.org/10.1371/journal.pbio.3001237
20. Case DA, Belfon K & Ben-Shalom IY, et al. 2020. AMBER 2020. University of California, San Francisco.
21. Maier JA, Martinez C, Kasavajhala K, Wickstrom L, Hauser KE, Simmerling C. ff14SB: improving the accuracy of protein side chain and backbone parameters from ff99SB. *J Chem Theory Comput*. 2015;11(8):3696-3713. https://doi.org/10.1021/acs.jctc.5b00255
22. Jorgensen WL, Chandrasekhar J, Madura JD, Impey RW, Klein ML. Comparison of simple potential functions for

simulating liquid water. *J Chem Phys*. 1983;79(2):926-935. https://doi.org/10.1063/1.445869
23. Socher E, Sticht H, Horn AHC. The conformational stability of nonfibrillar amyloid-β peptide oligomers critically depends on the C-terminal peptide length. *ACS Chem Neurosci*. 2014;5(3):161-167. https://doi.org/10.1021/cn400208r
24. Götz AW, Williamson MJ, Xu D, Poole D, Le Grand S, Walker RC. Routine microsecond molecular dynamics simulations with AMBER on GPUs. 1. Generalized Born. *J Chem Theory Comput*. 2012;8(5):1542-1555. https://doi.org/10.1021/ct200909j
25. Le Grand S, Götz AW, Walker RC. SPFP: Speed without compromise—a mixed precision model for GPU accelerated molecular dynamics simulations. *Comput Phys Commun*. 2013;184(2):374-380. https://doi.org/10.1016/j.cpc.2012.09.022
26. Salomon-Ferrer R, Götz AW, Poole D, Le Grand S, Walker RC. Routine microsecond molecular dynamics simulations with AMBER on GPUs. 2. Explicit solvent particle mesh Ewald. *J Chem Theory Comput*. 2013;9(9):3878-3888. https://doi.org/10.1021/ct400314y
27. Berendsen HJC, Postma JPM, van Gunsteren WF, DiNola A, Haak JR. Molecular dynamics with coupling to an external bath. *J Chem Phys*. 1984;81(8):3684-3690. https://doi.org/10.1063/1.448118
28. Ryckaert J-P, Ciccotti G, Berendsen HJC. Numerical integration of the cartesian equations of motion of a system with constraints: molecular dynamics of n-alkanes. *J Comput Phys*. 1977;23(3):327-341. https://doi.org/10.1016/0021-9991(77)90098-5
29. Hopkins CW, Le Grand S, Walker RC, Roitberg AE. Long-time-step molecular dynamics through hydrogen mass repartitioning. *J Chem Theory Comput*. 2015;11(4):1864-1874. https://doi.org/10.1021/ct5010406
30. Roe DR, Cheatham TE. PTRAJ and CPPTRAJ: software for processing and analysis of molecular dynamics trajectory data. *J Chem Theory Comput*. 2013;9(7):3084-3095. https://doi.org/10.1021/ct400341p
31. Schymkowitz J, Borg J, Stricher F, Nys R, Rousseau F, Serrano L. The FoldX web server: an online force field. *Nucleic Acids Res*. 2005;33(web server issue):W382-W388. https://doi.org/10.1093/nar/gki387
32. Pettersen EF, Goddard TD, Huang CC, et al. UCSF Chimera—a visualization system for exploratory research and analysis. *J Comput Chem*. 2004;25(13):1605-1612. https://doi.org/10.1002/jcc.20084
33. Wan Y, Shang J, Graham R, Baric RS, Li F. Receptor recognition by the novel coronavirus from Wuhan: an analysis based on decade-long structural studies of SARS coronavirus. *J Virol*. 2020;94(7):e00127-20. https://doi.org/10.1128/JVI.00127-20
34. Linsky TW, Vergara R, Codina N, et al. De novo design of potent and resilient hACE2 decoys to neutralize SARS-CoV-2. *Science*. 2020;370(6521):1208-1214. https://doi.org/10.1126/science.abe0075
35. Salleh MZ, Derrick JP, Deris ZZ. Structural evaluation of the spike glycoprotein variants on SARS-CoV-2 transmission and immune evasion. *Int J Mol Sci*. 2021;22(14):7425. https://doi.org/10.3390/ijms22147425
36. Starr TN, Greaney AJ, Hilton SK, et al. Deep mutational scanning of SARS-CoV-2 receptor binding domain reveals constraints on folding and ACE2 binding. *Cell*. 2020;182(5):1295-1310. https://doi.org/10.1016/j.cell.2020.08.012
37. Chan KK, Tan TJC, Narayanan KK, Procko E. An engineered decoy receptor for SARS-CoV-2 broadly binds protein S sequence variants. *Sci Adv*. 2021;7(8):eabf1738. https://doi.org/10.1126/sciadv.abf1738
38. Chakraborty S. Evolutionary and structural analysis elucidates mutations on SARS-CoV2 spike protein with altered human ACE2 binding affinity. *Biochem Biophys Res Commun*. 2021;534:374-380. https://doi.org/10.1016/j.bbrc.2020.11.075
39. Cheng MH, Krieger JM, Kaynak B, Arditi M, Bahar I. Impact of South African 501.V2 variant on SARS-CoV-2 spike infectivity and neutralization: a structure-based computational assessment. *bioRxiv*. 2021. https://doi.org/10.1101/2021.01.10.426143
40. Sharma T, Baig MH, Rahim M, Dong JJ, Cho J-Y. Unbuttoning the impact of N501Y mutant RBD on viral entry mechanism: A computational insight. *bioRxiv*. 2021. https://doi.org/10.1101/2020.12.30.424906
41. Singh J, Samal J, Kumar V, et al. Structure-function analyses of new SARS-CoV-2 variants B.1.1.7, B.1.351 and B.1.1.28.1: clinical, diagnostic, therapeutic and public health implications. *Viruses*. 2021;13(3):439. https://doi.org/10.3390/v13030439
42. Dehury B, Raina V, Misra N, Suar M. Effect of mutation on structure, function and dynamics of receptor-binding domain of human SARS-CoV-2 with host cell receptor ACE2: a molecular dynamics simulations study. *J Biomol Struct Dyn*. 2020:1-15. https://doi.org/10.1080/07391102.2020.1802348
43. Qiao B, La Olvera de Cruz M. Enhanced binding of SARS-CoV-2 spike protein to receptor by distal polybasic cleavage sites. *ACS Nano*. 2020;14(8):10616-10623. https://doi.org/10.1021/acsnano.0c04798

SUPPORTING INFORMATION

Additional Supporting Information may be found online in the supporting information tab for this article.

How to cite this article: Socher E, Conrad M, Heger L, et al. Computational decomposition reveals reshaping of the SARS-CoV-2–ACE2 interface among viral variants expressing the N501Y mutation. *J Cell Biochem*. 2021;122:1863-1872. https://doi.org/10.1002/jcb.30142